Preparation and Characterization of Aluminum Oxide–Poly(ethylene-*co*-butyl acrylate) Nanocomposites

P. Nordell,[1] S. Nawaz,[1] B. Azhdar,[1] H. Hillborg,[1,2] U. W. Gedde[1]

[1]*School of Chemical Science and Engineering, Fibre and Polymer Technology, Royal Institute of Technology, SE-100 44 Stockholm, Sweden*
[2]*ABB Corporate Research, Power Technology, SE–721 78 Västerås, Sweden*

Received 6 July 2011; accepted 23 September 2011
DOI 10.1002/app.36331
Published online 29 December 2011 in Wiley Online Library (wileyonlinelibrary.com).

ABSTRACT: This article describes the preparation and characterization of composites containing poly(ethylene-*co*-butyl acrylate) (EBA–13 and EBA–28 with 13 and 28 wt % butyl acrylate, respectively) and 2–12 wt % (0.5–3 vol %) of aluminum oxide nanoparticles (two types differing in specific surface area and hydroxyl-group concentration; uncoated and coated with, respectively, octyltriethoxysilane and aminopropyltriethoxysilane). A greater surface coverage was obtained with aminopropyltriethoxysilane than with octyltriethoxysilane. An overall good dispersion was obtained in the EBA-13 composites prepared by extrusion compounding. Composites with octyltriethoxysilane-coated nanoparticles showed the best dispersion. The addition of the nanoparticles to EBA–28 resulted in poor dispersion, probably due to insufficiently high shear forces acting during extrusion mixing which were unable to break down nanoparticle agglomerates. The nanoparticles had no effect on the crystallization kinetics in the EBA–13 composites, but in the EBA–28 composites the presence of the nanoparticles led to an increase in the crystallization peak temperature, suggesting that the nanoparticles had a nucleating effect in this particular polymer. © 2011 Wiley Periodicals, Inc. J Appl Polym Sci 125: 975–983, 2012

Key words: poly(ethylene-*co*-butyl acrylate); aluminum oxide nanoparticles; nanocomposites; silanization; dispersion; crystallization

INTRODUCTION

Polymer composites based on nanometer-sized inorganic filler particles have developed strongly since the pioneering work at the Toyota Company, Japan, which led to the commercialization of polyamide-6/clay nanocomposites in 1990.[1] One potential application of polymer nanocomposites is as an electrical insulating material.[2,3] It has been reported that the addition of inorganic nanoparticles gives a higher resistance toward partial discharges in a wide range of polymers including polyamides, polyimides, epoxy, and silicone rubber.[4–8] A higher breakdown strength, and/or voltage endurance, particularly at moderate field strengths, was observed for thermoplastics (isotactic polypropylene, ethylene-vinyl acetate copolymer and low-density polyethylene) and thermosets (epoxy) filled with a variety of nanoparticles.[9–15] A decrease in permittivity as a result of the addition of inorganic nanoparticles to polymers has also been reported, which is different from the behavior shown by composites based on micrometer-sized fillers.[16,17] It has been suggested that this unexpected effect was due to the large surface of the nanoparticles, yielding a large volume fraction of bound polymer layer with reduced segmental mobility. Related effects were observed for the loss factor (tan δ), which was strongly suppressed in epoxy–clay nanocomposites, particularly at higher temperatures.[16] It has now been established that these interesting results are controlled by the physics and chemistry of the large interfacial area of the nanoparticles, influencing the surrounding polymer matrix.[18] To benefit from the unique properties of nanocomposites, a good and reproducible dispersion of the nanoparticles in the polymer matrix is desirable. Unfortunately, the high surface-to-volume ratios found on the nanoscale often favor particle attraction and subsequent agglomeration. The challenge of dispersion control can be addressed via the elaboration of new process techniques in combination with reliable characterization methodologies. It is fair to state that the degree of dispersion at various stages in the process dictates the final structure and material properties.[19–22] This article presents a process for the manufacture of well-dispersed polymer nanocomposites based on pure or silanized aluminum oxide nanoparticles in poly(ethylene-*co*-butyl acrylate).

Correspondence to: U. W. Gedde (gedde@polymer.kth.se).
Contract grant sponsor: Elforsk; contract grant number: 63212.
Contract grant sponsor: Swedish Research Council; contract grant number: IFA 2007-5095.

This polymer is widely used in several branches including electrical industry as insulating and semiconductive layers in cables. Poly(ethylene-*co*-butyl acrylate) has the good properties of low-density polyethylene (produced by the high-pressure process), i.e., melt strength and toughness and the polarity of the butyl acrylate units offers better adhesive properties than low-density polyethylene. This article presents examples of composites with uniformly distributed nanoparticles together with examples of "failures," i.e., composites with poorly dispersed nanoparticles. The water uptake and the interaction between phenolic antioxidants and uncoated and coated nanoparticles are reported in two follow-up articles.[23,24]

EXPERIMENTAL

Materials

Poly(ethylene-*co*-butyl acrylate)s with either 13 or 28 wt % of butyl acrylate (referred to as EBA–13 or EBA–28, respectively) were supplied by Borealis AB, Stenungsund, Sweden. The butyl acrylate content was determined by infrared spectroscopy. The densities of EBA–13 and EBA–28 were 924 and 926 kg m^{-3}, respectively. The melt flow indices were 1.1 g/10 min (EBA–13) and 4 g/10 min (EBA–28), according to ISO 1133 (190°C, 2.16 kg weight).

Two types of aluminum oxide nanoparticles were used. Nanodur (ND) supplied by Nanophase, was a 70 : 30 δ : γ-phase aluminum oxide with an average particle diameter of 45 nm and a specific surface area of 45 m^2 g^{-1}. Nanoamor (NA) supplied by Nanostructured and Amorphous Materials, was a γ-Al_2O_3 with an average particle diameter of 25 nm and a specific surface area of 190 m^2 g^{-1}. The manufacturers provided all data concerning the aluminum oxide grades. The stabilizer Irganox 1010 (Ciba Specialty Chemicals, Switzerland) and the silane coupling agents—aminopropyltriethoxysilane (Sigma Aldrich) and octyltriethoxysilane (Fluka)—were used as received.

Nanoparticle characterization

Transmission electron micrographs of the nanoparticles were obtained using a Tecnai 10 transmission electron microscope operated at 80 kV. Samples were prepared by dissolving nanoparticles in ethanol using ultrasonication for 5 min, followed by collection onto a copper grid. The specific surface area of the different nanofillers were determined by measuring the nitrogen desorption isotherm using a BET FlowSorb II 2300 (Micromeritics) instrument in a single point area mode. The instrument was calibrated using a kaolinite standard (Micromeritics). A Mettler-Toledo SDTA thermogravimetric analyzer (TGA) 851 thermobalance equipped with a water cooler was used to obtain the mass loss of the nanoparticles before and after surface treatment. Samples weighing 5 ± 0.5 mg were placed in 70-μL alumina holders and heated from 25 to 800°C in oxygen at a rate of 10°C min^{-1}. All samples were dried under reduced pressure (0.5 kPa) at 50°C for 24 h before thermogravimetry. The hygroscopic behavior, i.e., the moisture uptake of the nanoparticles, was also determined gravimetrically using a Precisa XR 205 SM-DR balance.

Silanization of nanoparticles

The aluminum oxide nanoparticles were vacuum dried (0.5 kPa) for 24 h at 190°C to remove adsorbed water before surface treatment. The silanization procedure was as follows: (i) addition of 80 g of dried nanoparticles to 4000 mL of methanol/water (25 : 75 vol %), (ii) mechanical stirring for 15 min (iii), dropwise addition of silane under ultrasonication using a wand (300 W; Sonics Vibra Cell VCX 750) for 10 min, (iv) vigorous mechanical stirring for 4 h. For silanization of ND, 130 mL of each silane was added to 80 g of particles. In the case of NA, 300 mL of each silane was added due to the higher specific surface area of this nanofiller. To promote hydrolysis of octyltriethoxysilane, the pH was adjusted to 4.5 by the addition of acetic acid, in combination with an extension of the reaction time from 4 to 24 h. After the elapsed reaction time, the particles were collected by centrifugation in a Hettich bench centrifuge at 4500 rpm. The nanoparticles were washed in ethanol and isopropanol before final drying. The coated nanoparticles were dried at 110°C for 24 h, ground with pestle and mortar, and finally vacuum dried at 60°C for 24 h.

Manufacture of nanocomposites

EBA pellets were cryoground down to a particle size of 0.5 mm and then in a second step to 0.25 mm. Slurries of unmodified or silanized particles in ~ 10 wt % of isopropanol of the total mass, together with 0.2 wt % of stabilizer (Irganox 1010), were ultrasonicated (300 W; Sonics Vibra Cell VCX 750) in combination with magnetic stirring for 30 min to break up particle agglomerates. Each particle solution was mixed with the finely ground polymer in a three-dimensional (3D) ultramixer (Turbula Shaker Mixer Type T2F, WAG, Switzerland) at room temperature for 3 h. Subsequently, the mixture was sieved to 0.25 mm to eliminate large agglomerates before it was dried at 70°C for 30 min in a vacuum oven. The powder was then placed in the 3D mixer a second time for 2 h. All batches were finally vacuum dried at 50°C for 24 h and thereafter kept under vacuum in sealed glass flasks until the compounding. The

powder obtained was melt-compounded in a Prism Eurolab 16 XL twin-screw extruder (Thermo Electron Corporation), accompanied by a Prism Eurolab traditional strand pelletizer (set at 2.5-mm pellet length). The temperature profile was varied between 145 and 170°C (feeder to die) for the EBA–28 materials and between 160 and 195°C for the EBA–13 materials. The screw rotational speed was varied from 20 to 60 rpm. The torque varied from 10 to 24 Nm. The pellets were then extruded to tape-shaped films in a laboratory extruder (Plasticorder PL 2000, Brabender OHG, Duisburg, Germany), equipped with a screw of 19 mm diameter and L/D = 25. The temperature profile was 150–160°C (feeder) and 170°C (die). A ribbon die head, 100 × 1.5 mm, was used. The screw rotational speed was kept at 40 rpm. All tape-shaped films were finally dried in a vacuum oven at 50°C for 24 h before further characterization. In total, 36 different nanocomposites were prepared: EBA–13 or EBA–28 filled with 2, 6, and 12 wt % aluminum oxide nanoparticles (ND or NA) either uncoated (U) or coated with aminopropyltriethoxysilane (A) or with octyltriethoxysilane (O). Two reference strands containing only EBA–13 or EBA–28 and 0.2 wt % Irganox 1010 were prepared.

Characterization of nanocomposites

The thermal characteristics of the nanocomposites were assessed using a Mettler Toledo DSC 1 differential scanning calorimeter with Mettler Toledo STARe software V9.2. Samples weighing between 15 and 30 mg in aluminum sample holders were heated from −80 to 170°C, cooled from 170 to −80°C, and then finally heated from −80 to 170°C. The scanning rates were ±10°C min^{-1}, and the atmosphere was nitrogen flowing at 50 mL min^{-1}. The particle dispersion in the polymer matrix was quantified by studies of freeze-fractured surfaces in a Hitachi S-4800 field emission scanning electron microscope (SEM). The samples were sputtered with a 5–10-nm thick conductive metal layer in an Agar high-resolution sputter coater (Model 208RH) before examination in the SEM.

RESULTS AND DISCUSSION

Characteristics of aluminum oxide nanoparticles

The specific surface area of the nanofillers were determined by nitrogen desorption measurements (BET). For two different batches of uncoated ND, the following values were obtained: specific surface area = 36 ± 1 and 42 ± 1 m^2 g^{-1}. The value provided by the manufacturer was 40 m^2 g^{-1}. For uncoated NA, a specific surface area value of 174 ± 5 m^2 g^{-1} was obtained, which is close to the value 180 m^2 g^{-1} given by the manufacturer. The coated ND fillers showed lower specific surface area values (octyltriethoxysilane-coated ND: 25 ± 1 m^2 g^{-1}; aminopropyltriethoxysilane-coated: 31 ± 1 m^2 g^{-1}) than the uncoated ND. These data thus suggest that some agglomeration of nanoparticles occurred during the coating process. However, it is possible that these agglomerates disintegrated in the subsequent melt-compounding step. The octyltriethoxysilane-coated NA showed an even a larger specific surface area than the uncoated NA, 193 ± 6 m^2 g^{-1} compared to 174 ± 5 m^2 g^{-1}.

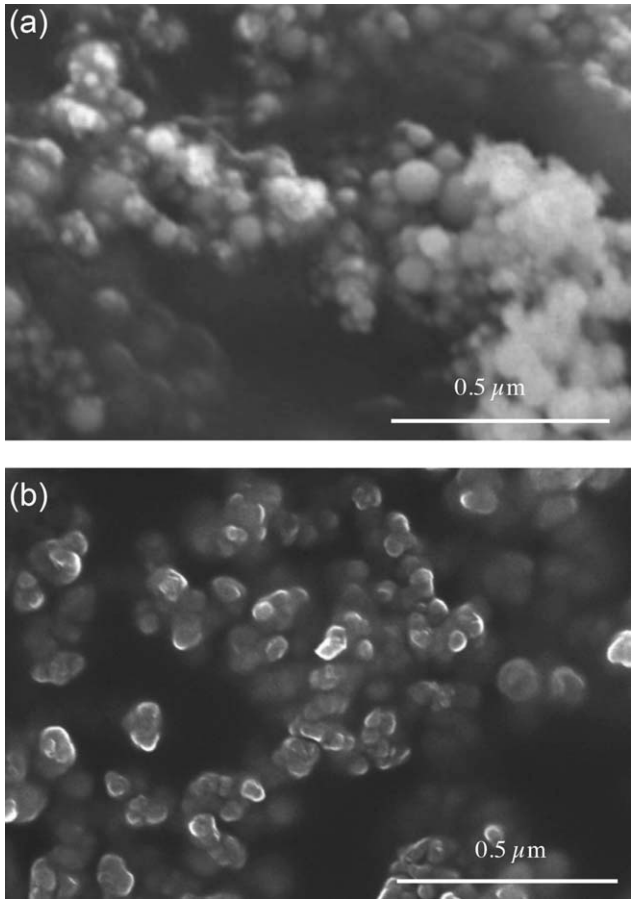

Figure 1 Scanning electron micrographs of the uncoated aluminum oxide nanoparticles showing (a) Nanodur and (b) Nanoamor.

The large surface-to-volume ratio of the nanoparticles led to a considerable adsorption of moisture due to interaction with the accessible hydroxyl groups on the nanoparticle surfaces. As the hydroxyl groups participate in the silanization reaction, it was desirable to remove the adsorbed water. This was done by carefully drying the particles according to the method described by Schadler et al.[25] The two types of aluminum oxide nanoparticles used in this study differed mainly in particle size and specific surface area, ~ 45 and 190 m^2 g^{-1}, respectively. SEM of the pristine nanoparticles are shown in Figure 1. ND consisted of spherical nanoparticles, whereas

TABLE I
Mass Loss and Silane Coverage of Nanoparticles

Nanofiller[a]	Mass loss (%)[b]	μmol Silane (m^{-2})[c]	X_{sil} (nm^{-2})[d]
NDU	0.1	0	0
NDO	0.5	0.7	0.4
NDA	0.7	2.2	1.4
NAU	8.9	0	0
NAO	13.6	2.3	1.4
NAA	13.3	4.2	2.5

[a] ND: Nanodur; NA: Nanoamor; last character being U: uncoated; O: treated with octyltriethoxysilane; A: treated with aminopropyltriethoxysilane.
[b] Mass loss percentage at 800°C with reference to the mass at 25°C obtained by thermogravimetry.
[c] Calculated coverage of nanoparticles with coating expressed in moles per unit area of particle surface. Displayed values were obtained from the mass loss data obtained by thermogravimetry.
[d] Calculated number of silane molecules per square nanometer of particle surface area. Displayed values were obtained from the mass loss data obtained by thermogravimetry.

NA consisted of equiaxial, irregular nanoparticles. The sorption of moisture by fully dried uncoated nanoparticles at 50% RH and 20°C resulted in weight gains of 0.4% (ND) and 7.9% (NA). The high-surface area particles (NA) adsorbed almost five times more moisture per unit surface area than the ND particles. It is suggested that the amount of adsorbed moisture was related to the number of available surface hydroxyl groups, and hence, this indicated that NA contained about five times more hydroxyl groups per unit surface area than ND.

The efficiency of silanization of the particles was assessed by thermogravimetry. Data for the weight loss of silanized and uncoated nanoparticles at 800°C, as well as the calculated surface coverage of silane, are presented in Table I. The calculations are based on the assumption that the silane hydrolyzed completely and that the difference in weight loss at 800°C between the silanized and uncoated particles was due to the complete elimination of the hydrocarbon components of the silanes. It was also assumed that the inorganic part of the silane (Si–O) was oxidized to silica.

The calculated graft density of aminopropyltriethoxysilane-coated ND, 2.2 μmol m^{-2} was lower than the previously reported value of 8.3 μmol m^{-2}.[26] The calculated graft density of the octyltriethoxysilane-coated ND was even lower, 0.7 μmol m^{-2}. These data thus indicate that the ND particles were only partially covered with silane. This finding was supported by transmission electron microscopy, which revealed weak cluster-like silane structures on the nanoparticle surfaces (indicated by arrows in Fig. 2).

NA exhibited a higher degree of surface coverage than ND, both for octyltriethoxysilane and aminopropyltriethoxysilane, 2.3 and 4.2 μmol m^{-2}, respectively. It is suggested that the high-hydroxyl group concentration in NA is responsible for the high graft density. For comparison, 4.8–7.5 μmol m^{-2} of 3-(trimetoxysilyl) propyl methacrylate was grafted onto different types of aluminum oxide.[27,28]

Dispersion of aluminum oxide nanoparticles in EBA

The filler loadings in the composites studied were 2, 6, and 12 wt %. This corresponds to volume fractions of 0.5, 1.5, and 3 vol %. In the following, the composites are primarily designated with their volume fractions because this quantity corresponds to the appearance of the particles in the fracture surfaces.

Figures 3 and 4 show SEM of fracture surfaces of the EBA–13/ND-composites obtained after immersion of specimens in liquid nitrogen. The nanoparticles are readily observed on the surfaces as almost spherical objects. Some nanoparticles appeared to be rather loosely bonded to the polymer matrix. Many of the particles visible in these composites were sitting in holes; the latter being of a larger diameter than the particle itself [Figs. 3(a–c)]. The composites containing octyltriethoxysilane-coated ND displayed mostly solitary particles and only a few smaller agglomerates of several particles. The composite with 3 vol % (12 wt %) of nanoparticles showed several two- and three-particle agglomerates [Fig. 3(b)]. In general, octyltriethoxysilane-coated ND was uniformly dispersed in EBA–13. The dispersion of uncoated ND in EBA–13 was good but a larger number of small agglomerates were nevertheless observed in this sample than in the composites with octyltriethoxysilane-coated ND [cf. Figs. 3(c) and

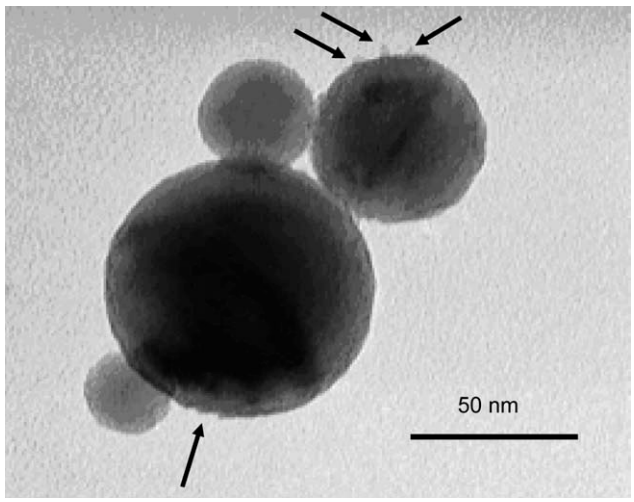

Figure 2 Transmission electron micrograph of ND nanoparticles coated with aminopropyltriethoxysilane. Note the protruding silane structures indicated by the arrows.

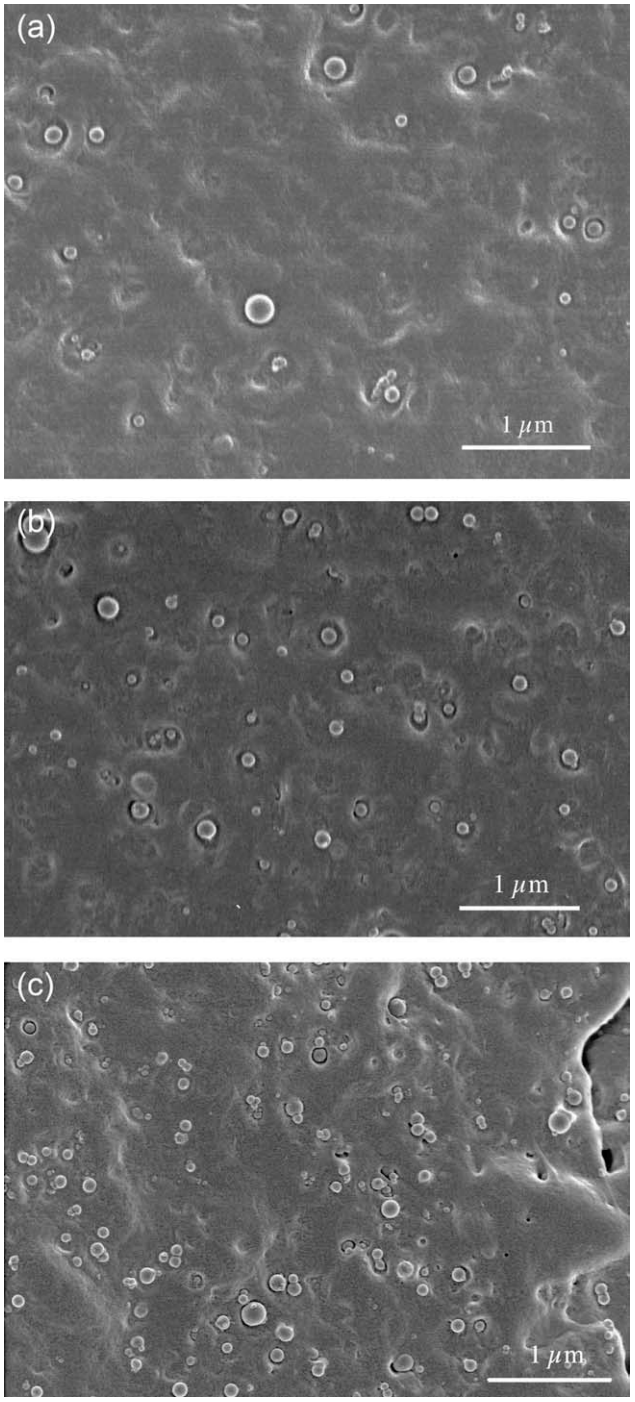

Figure 3 Scanning electron micrographs of fracture surfaces of composites based on EBA–13 and octyltriethoxysilane-coated ND with the following nanofiller contents: (a) 0.5 vol % (2 wt %); (b) 1.5 vol % (6 wt %); (c) 3 vol % (12 wt %).

4(a)]. The composites with aminopropyltriethoxysilane-coated nanoparticles showed a degree of dispersion intermediate between those of octyltriethoxysilane-coated ND and octyltriethoxysilane-uncoated ND [Fig. 4(b)]. The fibers present on the fracture surfaces were due to unwanted heating of the specimen prior to the cracking [Fig. 4(b)]. Composites based on EBA–13 and aminopropyltriethoxysilane-coated ND with other filler contents did not show these fibrous features, a fact that further substantiate the assumption that the fibrous structures found in Figure 4(b) are indeed "artificial" structures.

SEM covering a total surface area of ~ 2 mm^2 were screened in a search for nanoparticle dispersion and the presence of large agglomerates. The number of particles observed for each composite material was typically from 600 to 2000. The agglomerates were divided into six different categories: 1–5 particles together (Types 1–5) or >5 particles (Type 6). The results for the ND/EBA–13 are presented in histogram form in Figure 5. It is noteworthy that the even the Type 6 agglomerates were small in size (<300 nm), due to the fact that they consisted of one or two larger particles together with a few of the very smallest particles. The composites with 0.5 and 1.5 vol % filler showed similar dispersion levels. The number of solitary nanoparticles was significantly higher in these materials than in the composites with 3 vol % filler. The dispersion was optimal for the composites with 1.5 vol % filler. The dispersion was in general

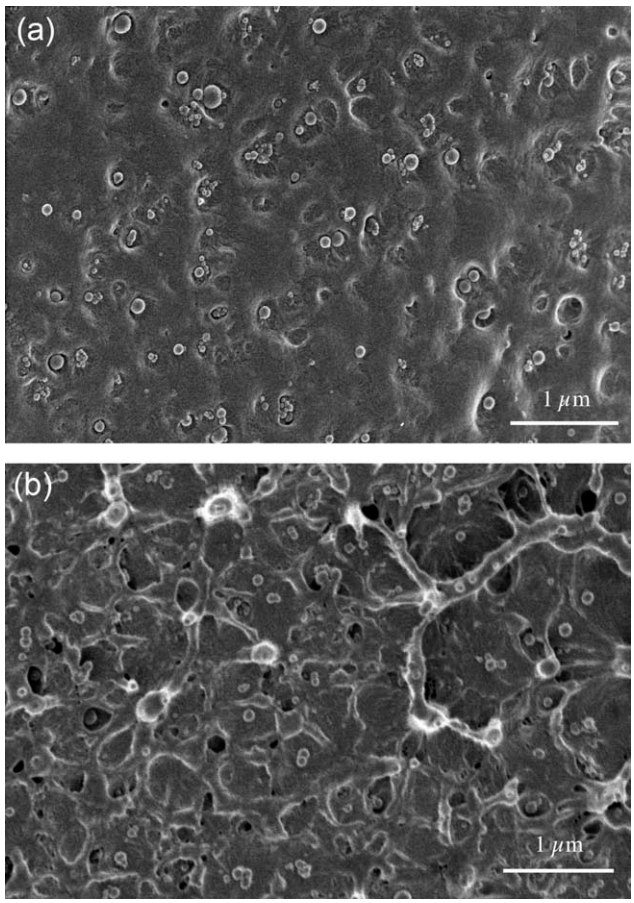

Figure 4 Scanning electron micrographs of fracture surfaces of EBA–13 composites containing: (a) 3 vol % (12 wt %) uncoated ND; (b) 3 vol % (12 wt %) aminopropyltriethoxysilane-coated ND.

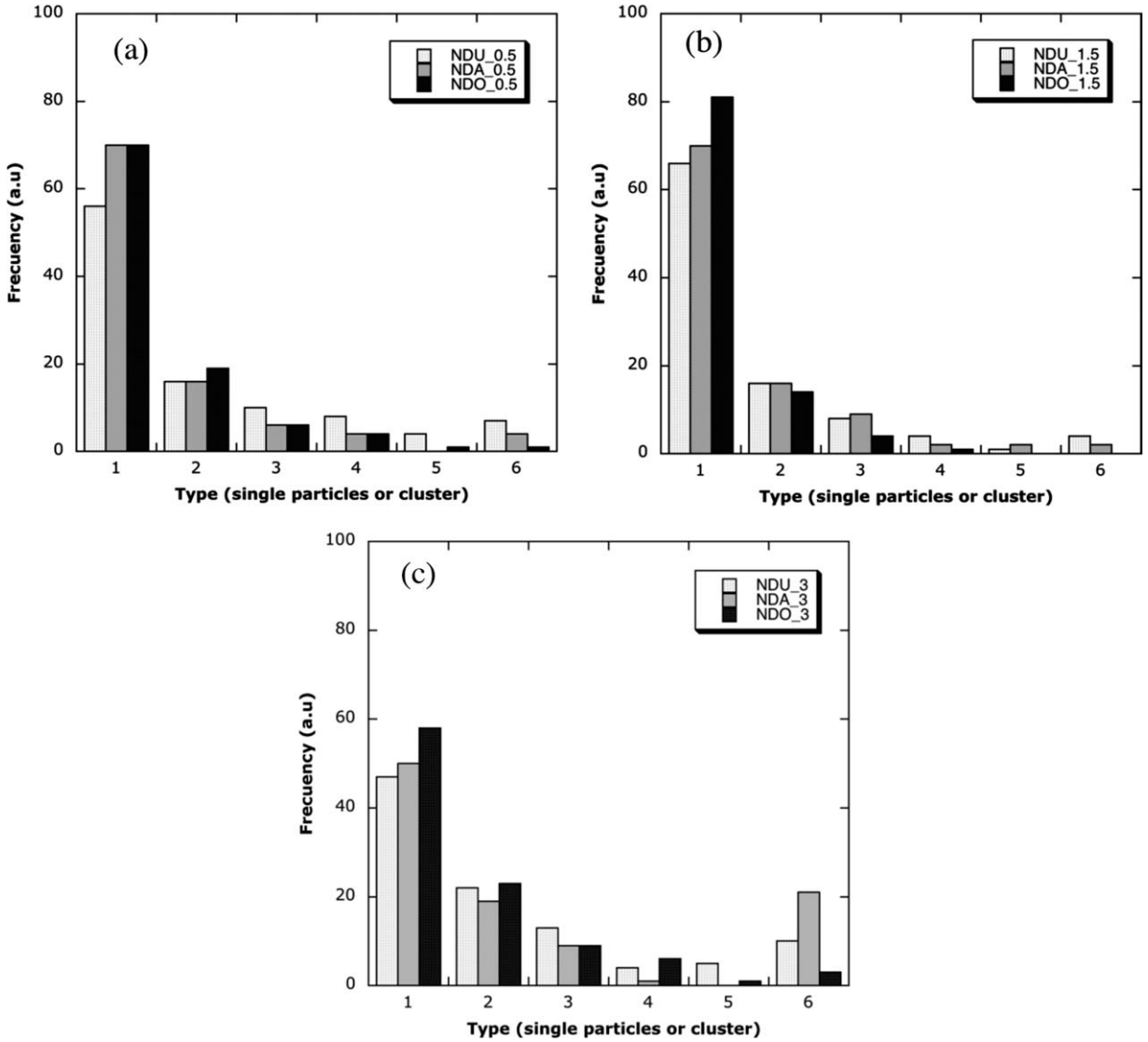

Figure 5 Distribution of numbers of particles in small agglomerates in the different ND/EBA–13 composites with the following filler contents: (a) 0.5 vol % (2 wt %); (b) 1.5 vol % (6 wt %); (c) 3 vol % (12 wt %). The different nanofillers are abbreviated as follows: NDU, uncoated ND; NDA, aminopropyltriethoxysilane-coated ND; NDO, octyltriethoxysilane-coated ND.

good for all materials containing the ND particles, although a few agglomerates 1–2 μm in size were observed in the composites with 0.5 and 1.5 vol % of untreated or aminopropyltriethoxysilane-coated particles. Silanization improved the dispersion, especially for the particles coated with octyltriethoxysilane. In fact, none of the materials containing these particles exhibited any μm-sized agglomerates, although some small clusters (<200 nm) were observed. This is probably due to the hydrophobic character of this silane, which prevents hydrogen bonding and the subsequent formation of hard agglomerates during the drying of the surface-treated particles.

The composites containing NA were evaluated in a different manner because of the particle irregularity and the difficulty in distinguishing individual particles (Fig. 6). The particles were instead categorized

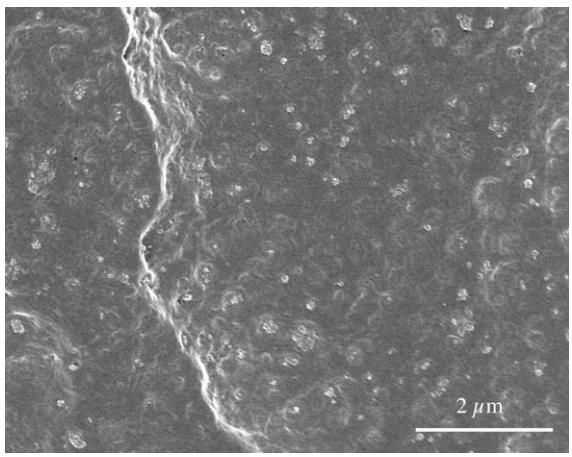

Figure 6 Scanning electron micrograph of fracture surface of EBA–13 composite containing 1.5 vol % (6 wt %) aminopropyltriethoxysilane-coated NA.

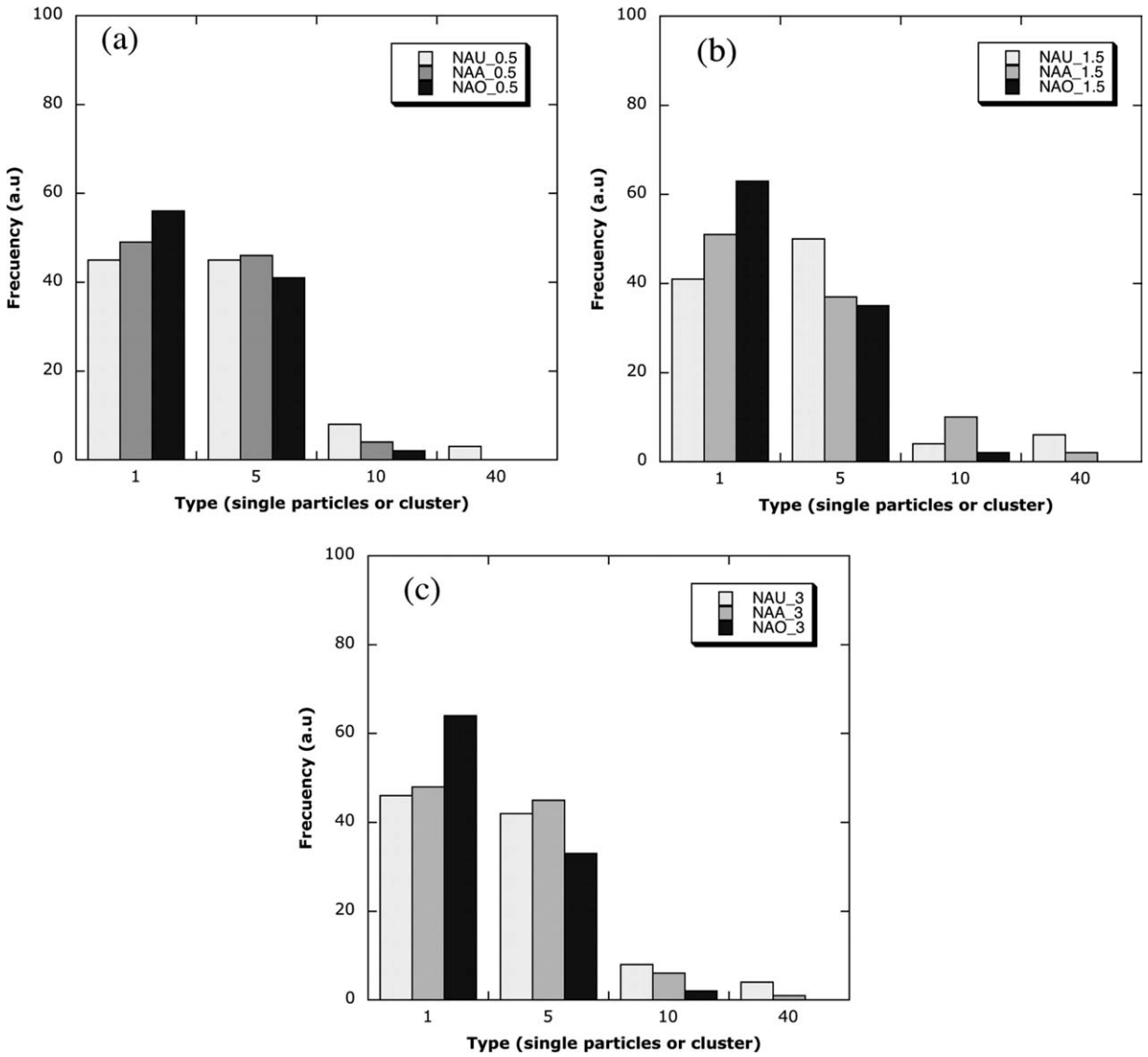

Figure 7 Distribution of number of particles in small agglomerates in the different NA/EBA–13 composites with the following filler contents: (a) 0.5 vol % (2 wt %); (b) 1.5 vol % (6 wt %); (c) 3 vol % (12 wt %). The different nanofillers are abbreviated as follows: NAU, uncoated NA; NAA, aminopropyltriethoxysilane-coated NA; NAO, octyltriethoxysilane-coated NA.

as: Type 1 (solitary particles), Type 5 (agglomerates consisting of 2–5 particles), Type 10 (agglomerates consisting of 6–10 particles), and Type 40 (agglomerates containing 11–40 particles). The results for NA/EBA-13 are summarized in Figure 7. The agglomerates in the NA/EBA–13 composites were larger and more frequent than in the composites based on ND and EBA-13, even though solitary particles also dominated also in the former materials. The best dispersion was found in materials with 0.5 vol % particles, although a few large agglomerates ($\sim$ 5 μm) were also found in these composites. Composites with larger loadings of NA contained even larger agglomerates.

Data for the average numbers of particles in the small agglomerates in the different EBA-13 composites are presented in Table II. The composites based on octyltriethoxysilane-coated ND showed the best dispersion, i.e., the fewest particles in the small agglomerates. The composites containing aminopropyltriethoxysilane-coated ND showed marginally higher average particle numbers, whereas composites containing uncoated ND showed a more significant increase in the average particle numbers. The NA composites displayed larger small agglomerate sizes than the ND composites. The least well-dispersed composite was that based on uncoated NA.

The composites based on EBA–28 exhibited poorly dispersed nanoparticles [Fig. 8(a,b)]. It is believed that this was due to the low melt viscosity of EBA–28 so that the shear forces during the extrusion mixing were insufficient to break up the nanoparticle agglomerates during the extrusion mixing. These materials were further characterized, even though they cannot be considered "true nanocomposites."

TABLE II
Average Number of Particles in Small Agglomerates in EBA–13 Composites[a]

Nanofiller[b]	2 wt %	6 wt %	12 wt %
NDU	3.4	2.6	3.5
NDO	2.1	1.5	2.6
NDA	2.5	2.4	4.1
NAU	15.0	21.0	18.0
NAO	3.2	3.1	3.1
NAA	3.7	13.0	8.8

[a] Average (number) of particles in small agglomerates as revealed by scanning electron microscopy.
[b] ND, Nanodur; NA, Nanoamor; U, uncoated; O, treated with octyltriethoxysilane; A, treated with aminopropyltriethoxysilane.

The only exception was the material based on octyltriethoxysilane-coated ND particles in EBA–28, a material that showed only relatively few large agglomerates and a morphology resembling that of the EBA–13 composites [Fig. 8(c)].

Thermal characterization of nanocomposites

The crystallinity (w_c) was determined according to the total enthalpy method:

$$w_c = \frac{\Delta h}{\Delta h_f^0(T_1)} \tag{1}$$

$$\Delta h_f^0(T_1) = \Delta h_f^0(T_m^0) - \int_{T_1}^{T_m^0} (c_{p,a} - c_{p,c})dT \tag{2}$$

where Δh is the heat of melting, Δh_f^0 (T_1) is the heat of melting of 100% polymer at the onset temperature of melting (T_1), Δh_f^0 (T_m^0) is the heat of melting of 100% polymer at the equilibrium melting temperature (T_m^0), and $c_{p,a}$ and $c_{p,c}$ are the heat capacities of the amorphous and crystalline components, respectively. The values were then normalized with respect to filler content. The crystallinity of the pure EBA–13 was calculated to 42 wt %. The EBA–13 composites showed crystallinities scattering $\sim$ 42 wt % with no systematic deviation with regard to filler type. The standard deviation including data from all composites was between 2 and 3 wt %. The same observation was made for the EBA–28 composites; the crystallinity data were all scattered (standard deviation = 2 wt %) about the crystallinity of the pristine polymer, 21 wt %.

The nanoparticles, especially ND, appeared to act as nucleation agents in EBA–28, leading to an increase in the crystallization temperature (Fig. 9). As crystallization at a higher temperature generally favors a higher final crystallinity, one would expect a higher crystallinity in the nanocomposites compared to that of the neat EBA–28. However, the crystallinity was essentially the same as in the neat material.

CONCLUSIONS

The processing of nanocomposites by converting the raw materials, i.e., nanoparticles, coating chemicals, antioxidant and poly(ethylene-*co*-butyl acrylate), into a composite material with a certain degree of

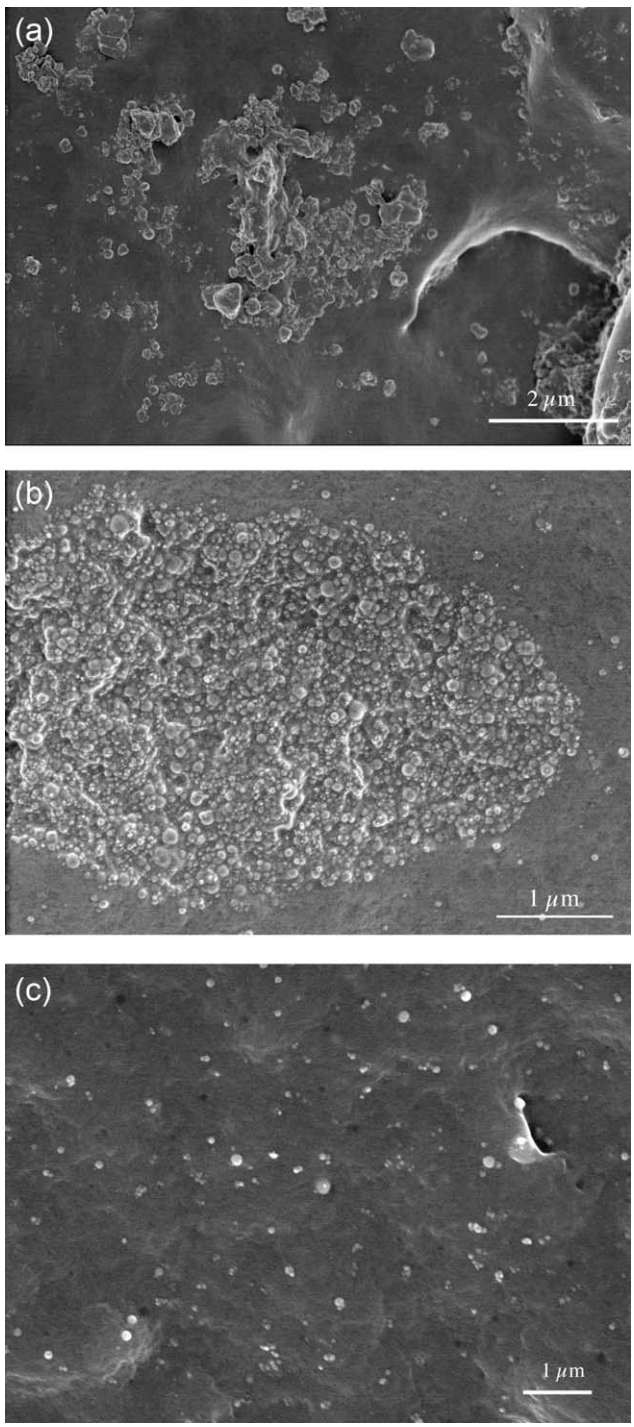

Figure 8 Scanning electron micrographs of fracture surfaces of the following EBA–28 composites with the following filler contents and fillers: (a) 0.5 vol % (2 wt %) uncoated NA; (b) 1.5 vol % (3 wt %) aminopropyltriethoxysilane-coated NA; (c) 1.5 vol % (3 wt %) octyltriethoxysilane-coated ND.

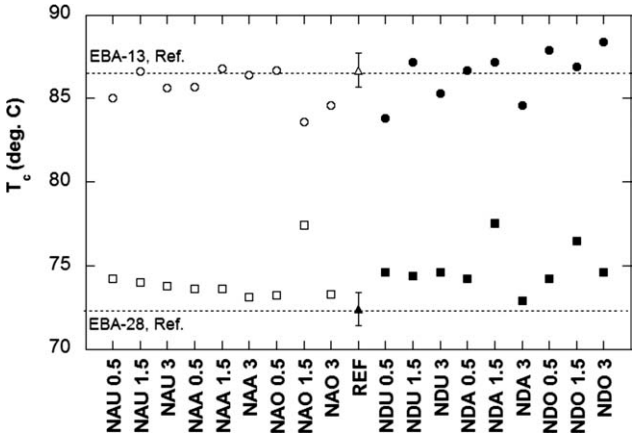

Figure 9 Crystallization peak temperatures for the different EBA-composites as shown in the graph. Abbreviations: REF, pristine polymers; NDU, uncoated ND; NDA, aminopropyltriethoxysilane-coated ND; NDO, octyltriethoxysilane-coated ND; NAU, uncoated NA; NAA, aminopropyltriethoxysilane-coated NA; NAO, octyltriethoxysilane-coated NA. The numbers displayed in the composite code refer to the volume percentage of nanofiller in the composite.

dispersion of the nanoparticles is the theme of this article. One of the polymers studied, poly(ethylene-*co*-butyl acrylate) with 13 wt % butyl acrylate, had a high melt viscosity (low-melt flow index) and the composites based on this polymer generally possessed good dispersion of the nanoparticles. The nanoparticle agglomerates, evidently present after surface coating, were fragmented by the shearing action of the polymer melt during extrusion compounding. The other polymer studied, poly(ethylene-*co*-butyl acrylate) with 28 wt % butyl acrylate, with a lower melt viscosity (higher melt flow index) was not able to break down the nanoparticle agglomerates because the shear stresses were insufficient. The two aluminum oxide nanoparticles used had different specific surface area (different by a factor of four) and different specific hydroxyl group concentrations (different by a factor of five). The nanoparticles with the greater specific surface area and higher specific hydroxyl group concentration more easily formed agglomerates; the attractive forces between the nanoparticles must be greater for this nanofiller than for the other nanofillers with lower specific surface area and hydroxyl group concentration. Surface coating using octyltriethoxysilane (resulting in a terminal octyl group) and aminopropyltriethoxysilane (resulting in a terminal amino group), although in neither case complete, decreased the attractive forces between nanoparticles and gave composites with better nanoparticle dispersion. In poly(ethylene-*co*-butyl acrylate) with 28 wt % butyl acrylate the nanoparticles acted as nucleation agents, increasing the crystallization temperature by several degrees.

Dr. Richard Olsson, Fibre and Polymer Technology, Royal Institute of Technology, is thanked for the transmission electron microscopy study.

References

1. Okada, O.; Kawakami, M.; Kojima, Y.; Kurauchi, T.; Kamigaito, O. Proc MRS Symp 1990, 171, 45.
2. Nelson, J. K.; Fothergill, J. C. Nanotechnology 2004, 15, 586.
3. Tanaka, T.; Kindersberger, J.; Fréchette, M. CIGRE Publication 451, 2011.
4. Kozaka, M.; Fuse, N.; Ohki, Y.; Okamoto, T.; Tanaka, T. IEEE Trans Dielectr Electr Insul 2005, 11, 833.
5. Fuse, N.; Kozaka, M.; Tanaka, T.; Murase, S.; Ohki, Y. Ann Report IEEE-CEIDP 2004, 4-4, 322.
6. Kozaka, M.; Kido, R.; Fuse, N.; Ohki, Y.; Okamoto, T.; Tanaka, T. Ann Report IEEE-CEIDP 2004, 5A-15, 398.
7. Kozako, M.; Yamano, S.; Kido, R.; Ohki, Y.; Kohtoh, M.; Okabe, S. Proc ISEIM 2005, 231.
8. Kozako, M.; Kido, R.; Imai, T.; Ozaki, T.; Shinizu, T.; Tanaka, T. Proc ISEIM 2005, 661.
9. Nelson, J. K.; Hu, Y. Ann Report IEEE-CEIDP 2003, 8-2, 719.
10. Nelson, J. K.; Hu, Y. Ann Report IEEE-CEIDP 2004, 7P-10, 832.
11. Zilg, C.; Kaempfer, D.; Mülhaupt, R.; Montanari, G. C. Ann Report IEEE-CEIDP 2003, 6-5, 546.
12. Imai, T.; Sawa, F.; Ozaki, T.; Nakano, T.; Shimizu, T.; Yoshimitsu, T. IEEE Trans A 2004, A-124, 11, 1064.
13. Ding, H. Z.; Varlow, B. R. Ann Report IEEE-CEIDP 2004, 4-6, 332.
14. Ma, D.; Siegel, R. W.; Hong, J. I.; Schadler, L. S.; Mårtensson, E.; Önneby, C. J Mater Res 2004, 19, 857.
15. Roy, M.; Nelson, J. K.; MacCrone, R. K.; Schadler, L. S. IEEE Trans Dielectr Electr Insul 2005, 12, 629.
16. Nelson J. K.; Utracki, L. A.; MacCrone, R. K.; Reed, C. W. Ann Report IEEE-CEIDP 2004, 4-2, 314.
17. Fothergill, J. C.; Nelson, J. K.; Fu, M. Ann Report IEEE-CEIDP 2004, 5A-17, 406.
18. Nelson, J. K.; Schadler, L. S. IEEE Trans Dielectr Electr Insul 2008, 15, 1.
19. Fiedler, B.; Gojny, F. H.; Wichmann, M. H. G.; Nolte, M. C. M.; Schulte, K. Comp Sci Tech 2006, 66, 3115.
20. Saltiel, C.; Chen, Q.; Manickavasagam, S.; Schadler, L. S.; Siegel, R. W.; Menguc, M. P. J Nanoparticle Res 2004, 6, 35.
21. Ton-That, M. T.; Perrin-Sarazin, F.; Cole, K. C.; Bureau, M. N.; Denault, J. Polym Eng Sci 2004, 44, 1212.
22. Tillekeratne, M.; Jollands, M.; Cser, F.; Bhattacharya, S. N. J Appl Polym Sci 2006, 100, 2652.
23. Nordell, P.; Nilsson, F.; Hedenqvist, M. S.; Hillborg, H.; Gedde, U. W. Eur Polym J, doi: 10.1016/j.eurpolymj.2011.09.013.
24. Nawaz, S.; Nordell, P.; Hillborg, H.; Gedde, U. W. Polym Degrad Stab, submitted.
25. Ma, D.; Siegel, R. W.; Hong, J. I.; Schadler, L. S. J Mater Res 2004, 19, 857.
26. Zhao, S.; Auletta, T.; Hillborg, H.; Schadler, L. S. Comp Sci Tech 2008, 68, 2965.
27. Baumgarten, E.; Wagner, R.; Lentes-Wagner, C.; Fresenius, Z. Anal Chem 1989, 334, 246.
28. Hall, W. K.; Lutinski, F. E.; Gerberich, H. R. J Catal 1964, 3, 512.